68Ga-PSMA-11 PET, 18F-PSMA-1007 PET, and MRI for gross tumor volume delineation in primary prostate cancer: intermodality and intertracer variability

Draulans, C.; Pos, F.; Smeenk, R.J.; Kerkmeijer, L.; Vogel, W.V.; Nagarajah, J.; ... ; Haustermans, K.

Practical Radiation Oncology® (2021) **11**, 202-211

practical radiation oncology®
pro
www.practicalradonc.org

Basic Original Report

^{68}Ga-PSMA-11 PET, ^{18}F-PSMA-1007 PET, and MRI for Gross Tumor Volume Delineation in Primary Prostate Cancer: Intermodality and Intertracer Variability

Cédric Draulans, MD, PhD,[a,b] Floris Pos, MD, PhD,[c] Robert J. Smeenk, MD, PhD,[d] Linda Kerkmeijer, MD, PhD,[d,e] Wouter V. Vogel, MD, PhD,[c,f] James Nagarajah, MD, PhD,[g] Marcel Janssen, MD, PhD,[g] Cindy Mai, MD [h] Stijn Heijmink, MD, PhD,[i] Marloes van der Leest, MD, PhD,[g] Patrik Zámecnik, MD, PhD,[g] Raymond Oyen, MD, PhD,[h] Sofie Isebaert, MSc, PhD,[a,b] Frederik Maes, MSc, PhD,[j,k] Steven Joniau, MD, PhD,[l,m] Martina Kunze-Busch, MSc, PhD,[d] Robin De Roover, MSc,[a,b] Gilles Defraene, MSc, PhD,[a,b] Uulke A. van der Heide, MSc, PhD,[c] Karolien Goffin, MD, PhD,[n,1] and Karin Haustermans, MD, PhD[a,b,*,1]

[a]Department of Radiation Oncology, University Hospitals Leuven, Leuven, Belgium; [b]Department of Oncology, KU Leuven, Leuven, Belgium; [c]Department of Radiation Oncology, The Netherlands Cancer Institute, Amsterdam, The Netherlands; [d]Department of Radiation Oncology, Radboud University Medical Center, Nijmegen, The Netherlands; [e]Department of Radiation Oncology, University Medical Centre, Utrecht, The Netherlands; [f]Department of Nuclear Medicine, The Netherlands Cancer Institute, Amsterdam, The Netherlands; [g]Department of Radiology & Nuclear Medicine, Radboud University Medical Centre, Nijmegen, The Netherlands; [h]Department of Radiology, University Hospitals Leuven, Leuven, Belgium; [i]Department of Radiology, The Netherlands Cancer Institute, Amsterdam, The Netherlands; [j]Department of Electrical Engineering, ESAT/PSI, KU Leuven, Leuven, Belgium; [k]Medical Imaging Research Centre, University Hospitals Leuven, Leuven, Belgium; [l]Department of Urology, University Hospitals Leuven, Leuven, Belgium; [m]Department of Development and Regeneration, KU Leuven, Leuven, Belgium; and [n]Department of Nuclear Medicine, University Hospitals Leuven, Leuven, Belgium

Received 10 January 2018; revised 11 October 2020; accepted 8 November 2020

Sources of support: This work had no specific funding.
Disclosures: All authors report having no conflict of interest related to the content of this manuscript.
Research data are stored in an institutional repository and will be shared upon request to the corresponding author.
* Corresponding author: Karin Haustermans, MD, PhD; E-mail: karin.haustermans@uzleuven.be
[1] K.G. and K.H. contributed equally to this work.

https://doi.org/10.1016/j.prro.2020.11.006

Abstract

Purpose: To assess the intermodality and intertracer variability of gallium-68 (^{68}Ga)- or fluorine-18 (^{18}F)-labeled prostate-specific membrane antigen (PSMA) positron emission tomography (PET) and biparametric magnetic resonance imaging (bpMRI)-based gross tumor volume (GTV) delineation for focal boosting in primary prostate cancer.

Methods: Nineteen prospectively enrolled patients with prostate cancer underwent a PSMA PET/MRI scan, divided into a 1:1 ratio between ^{68}Ga-PSMA-11 and ^{18}F-PSMA-1007, before radical prostatectomy (IWT140193). Four delineation teams performed manual contouring of the GTV based on bpMRI and PSMA PET imaging, separately. Index lesion coverage (overlap%) and interobserver variability were assessed. Furthermore, the distribution of the voxelwise normalized standardized uptake values (SUV%) was determined for the majority-voted (>50%) GTV (GTV^{majority}) and whole prostate gland to investigate intertracer variability. The median patientwise SUV% contrast ratio (SUV%-CR, calculated as median GTV^{majority} SUV% / median prostate gland without GTV^{majority} SUV%) was calculated according to the tracer used.

Results: A significant difference in overlap% favoring PSMA PET compared with bpMRI was found in the ^{18}F subgroup (median, 63.0% vs 53.1%; $P = .004$) but was not present in the ^{68}Ga subgroup (32.5% vs 50.6%; $P = .100$). Regarding interobserver variability, measured Sørensen-Dice coefficients (0.58 vs 0.72) and calculated mean distances to agreement (2.44 mm vs 1.22 mm) were statistically significantly lower and higher, respectively, for the ^{18}F cohort compared with the ^{68}Ga cohort. For the bpMRI-based delineations, the median Sørensen-Dice coefficient and mean distance to agreement were 0.63 and 1.76 mm, respectively. Median patientwise SUV %-CRs of 1.8 (interquartile range [IQR], 1.6-2.7) for ^{18}F-PSMA and 3.3 (IQR, 2.7-5.9) for ^{68}Ga-PSMA PET images were found.

Conclusions: Both MRI and PSMA PET provided consistent intraprostatic GTV lesion detection. However, the PSMA tracer seems to have a major influence on the contour characteristics, owing to an apparent difference in SUV% distribution in the prostate gland.

Introduction

External beam radiation therapy (EBRT) is a curative treatment option for patients diagnosed with prostate cancer (PCa). After EBRT for PCa, depending on the risk group, up to half of patients experience a biochemical recurrence within 10 years.[1] Among patients who relapse after EBRT, about 20% to 40% present an isolated local recurrence,[2] which usually originates at the site of the primary tumor.[3] Adding a focal boost to the dominant intraprostatic lesion(s) may improve disease control. This hypothesis is currently being tested in multiple clinical trials (eg, FLAME (Investigate the Benefit of a Focal Lesion Ablative Microboost in ProstatE Cancer) [NCT01168479][4] and DELINEATE [ISRCTN04483921][5]). In these focal boosting trials, the gross tumor volume (GTV) delineation is generally defined on magnetic resonance imaging (MRI), using primarily T2-weighted (T2w) imaging and diffusion-weighted imaging (DWI).

During the past few years, radioactively labeled tracers targeting the prostate-specific membrane antigen (PSMA) for positron emission tomography (PET) have been increasingly used in cases of biochemical recurrence after primary therapy to detect the site of recurrence. These tracers are small molecular inhibitors of PSMA that bind with the extracellular site of PSMA and can be labeled with the positron-emitting radioisotopes gallium-68 (^{68}Ga) or fluorine-18 (^{18}F). ^{18}F has a longer half-life, increased positron yield, and shorter positron range compared with ^{68}Ga. The role of PSMA PET in the detection of primary PCa is currently under investigation. PSMA PET already demonstrated a high diagnostic accuracy and a good correlation with gold standard histopathology in terms of lesion detection.[6-9] In addition, highly comparable sensitivity and specificity were shown in the detection of primary PCa using both MRI and PSMA PET / computed tomography (CT).[10]

Considering the promising findings of the use of PSMA PET in the detection of intraprostatic lesions, the interest in the use of this modality for focal boost delineation is growing.[11,12] This being said, the accuracy in detection of index lesions is not the only factor influencing the applicability of an imaging technique for GTV delineation. In addition, delineation-based target-volume covering as well as the magnitude of observer variability also strongly influence the applicability of certain imaging techniques for radiation therapy delineation purposes in daily clinical practice.

The goal of this study was therefore to compare PSMA PET with the current standard MRI for intraprostatic GTV delineation for focal boosting, regarding both target-volume covering and observer variability. Furthermore, another aim of this trial was to assess if ^{68}Ga-PSMA-11 and ^{18}F-PSMA-1007 are fully exchangeable in light of PSMA PET-based GTV delineations without any consequences in PCa patients.

Methods and Materials

Patient Population

This study was approved by the institutional ethical review board of the University Hospitals Leuven (UZL) (S62183). Twenty patients who were prospectively included in a trial investigating high-precision imaging of PSMA for personalized treatment in PCa (NCT03327675) between October 2017 and May 2019 were selected to assess the variability between ^{68}Ga-

PMSA-11 PET, ^{18}F-PSMA-1007 PET, and biparametric MRI (bpMRI)−based GTV delineations. Inclusion criteria for this trial were male sex, age between 18 and 75 years, and a histologically confirmed diagnosis of adenocarcinoma of the prostate. Only patients with high-risk or intermediate-risk PCa and a 5% or greater likelihood of lymph node invasion according to the Briganti nomogram were eligible for this trial.[13] Furthermore, for trial inclusion, patients had to be scheduled to undergo radical prostatectomy with an extended pelvic lymph node dissection. If involvement of pelvic lymph nodes was expected based on the preoperative diagnostic MRI information or if bone metastases were found on the staging bone scintigraphy, patients were excluded. In addition, patients who had undergone previous pelvic irradiation, patients with a World Health Organization performance status >2, or patients diagnosed with another malignancy during the previous 5 years were ineligible for trial inclusion. Written informed consent was obtained from all patients.

PET/MR Imaging

PET/MR imaging was performed on the GE SignaTM PET/MRI system (GE Healthcare, Waukesha, Wisconsin). All patients underwent a whole-body ^{68}Ga-PSMA-11 or ^{18}F-PSMA-1007 PET scan at 60 minutes post-injection. The patients were divided in a 1:1 ratio between ^{68}Ga-PSMA-11 and ^{18}F-PSMA-1007. The ^{68}Ga-PSMA-11 was produced on site as described previously using $^{68}Ga^{3+}$ obtained from a ^{68}Ge/^{68}Ga radionuclide generator (Eckert & Ziegler Radiopharma, Berlin, Germany).[14] The ^{18}F-PSMA-1007 was generated on site using an AllInOne synthesis module (Trasis SA, Ans, Belgium), reagent kit, and precursor for PSMA-1007 (ABX Advanced Biochemical Compounds GmbH, Radeberg, Germany) and ^{18}F from an in-house cyclotron. The uptake of PSMA was quantified in terms of standardized uptake values (SUV; regional tracer concentration normalized by the injected activity and body weight). Subsequently, an SUV % was determined per voxel by converting each SUV to a percentage relative to the highest SUV measured in the corresponding prostate and seminal vesicles. Simultaneously with the PET scan, an MRI scan including T2w imaging, DWI, and T1-weighted (T1w) imaging of the prostate and pelvis was performed. Apparent diffusion coefficient (ADC) maps were calculated from the DWI scan. A summary of the imaging sequences and parameters is given in Table EA.

Delineation

Twelve delineators were divided into 4 delineation teams in 3 centers. Each team consisted of a radiation oncologist, a nuclear medicine physician experienced in PSMA PET, and a radiologist experienced in uro-oncology (NKI-AvL: FP, WV & SH; UZL: KH, KG & CM; Radboud-1: RJS, MvdL & JN; Radboud-2: LK, PZ & MJ). All radiation oncologists had experience in the delineation of intraprostatic nodule(s) during the previously performed phase III FLAME and phase II hypo-FLAME trials conducted by the FLAME consortium.[15,16] Axial T2w and DWI images were read side by side, and visible tumors were delineated on the transversal T2w planes by the radiation oncologist jointly with the radiologist of each team. Similarly, suspect visible lesions were delineated on the PSMA PET images, linked to the T1w images only for anatomic correlation, by the radiation oncologist in collaboration with the nuclear medicine physician. A union volume (bpMRI ∪ PSMA PET) and intersection volume (bpMRI ∩ PSMA PET) were created for each patient using MIM, version 6.8.5 (MIM Software Inc, Cleveland, Ohio). Furthermore, a majority-voted PET-based GTV ($GTV^{majority}$) was created to which voxels did or did not belong, according to the results of the majority (>50%) of the individual PSMA PET-based segmentations. The "doubtful" GTV region ($GTV^{minority}$) was created by subtracting the majority-voted GTV from the merged GTV, which unified the contours of the 4 delineation teams. To simulate a realistic clinical situation, biopsy information and written radiology reports of the diagnostic MRIs were available. All teams used the delineation system of their own hospital (NKI-AvL: Mirada RTx, version 1.2.0.59, Mirada Medical Ltd, Oxford, United Kingdom; UZL: MIM, version 6.8.5, MIM Software Inc, Cleveland, Ohio; and Radboud-1 & 2: Pinnacle, version 16.0, Philips, Eindhoven, The Netherlands).

Histopathology and Image Registration

The radical prostatectomy specimens were inked to allow proper orientation and sectioned at 3-mm to 4-mm intervals perpendicular to the urethra. These whole-mount histologic slices were stained with hematoxylin and eosin (H&E). Afterward, the tumor lesions were delineated by a uropathologist. The pathologic tumor category (pT), Gleason pattern, and International Society of Urological Pathology (ISUP) grade group were determined for each tumor lesion according to the pT classification of the Union for International Cancer Control, eighth edition, and the ISUP 2014 modified grading system, respectively.[17,18] Conventionally, the histopathologic index lesion was defined as the largest lesion with the highest assigned ISUP grade group within each patient.[19,20]

The H&E slides were registered to the T2w MRI image to estimate the index lesion detection accuracy across the different image modalities used. For this purpose, each T2w MRI slice was assigned to the best-

Table 1 Terminology

Term	Definition
$GTV^{majority}$	A majority-voted PET-based GTV ($GTV^{majority}$) was created to which voxels did or did not belong, according to the results of the majority (>50%) of the individual PSMA PET-based segmentations.
$GTV^{minority}$	The "doubtful" GTV region ($GTV^{minority}$) was created by subtracting the majority-voted GTV from the merged GTV, which unified the contours of the 4 delineation teams.
Overlap%	The spatial overlap of the image-based delineation with the pathologically determined index lesion was reported as a percentage of overlap relative to the volume of the index lesion delineated by the uropathologist and registered to the images.
Sørensen-Dice coefficient (DSC)	The DSC was calculated by dividing 2 times the overlap volume by the sum of the 2 volumes.
Mean distance to agreement (MDA)	To evaluate the variability between the contour borders independent of the GTV, the MDA was calculated. The MDA measured the mean of the distances of each point on the contour surface to the closest point on the other contour.
Voxelwise normalized SUV (SUV%)	The SUV% was determined per voxel by converting each SUV to a percentage relative to the highest SUV measured in the corresponding prostate and seminal vesicles.
SUV% contrast ratio (SUV%-CR)	The SUV%-CR was calculated by dividing the median $GTV^{majority}$ SUV% to the median (prostate gland − $GTV^{majority}$) SUV%.

Abbreviations: GTV = gross tumor volume; PSMA = prostate-specific membrane antigen; PET = positron emission tomography; SUV = standard uptake value.

matching H&E slide based on the relative order of the H&E slides. For some T2w slices, no matching H&E slide was available, as the extremities of the apex and base of the prostate were removed and cut in a sagittal direction. The H&E slides were registered to T2w slices making use of a deformable point-based registration in MATLAB, R2019a (MathWorks, Natick, MA). This registration was based on prostate boundary and intraprostatic landmarks (median, 12 landmarks/slide; interquartile range [IQR], 10-15 landmarks/slide) and was visually checked.

Statistical Analysis

To quantify the accuracy in index-lesion detection, index lesions were defined as nondetected if the delineation contour did not intersect the pathologically determined index lesion. Furthermore, the spatial overlap of the image-based delineation with the pathologically determined index lesion was reported as a percentage of overlap relative to the volume of the index lesion delineated by the uropathologist and registered to the images (overlap%). To quantify interobserver variability, the Sørensen-Dice coefficient (DSC) and mean distance to agreement (MDA) of the contours were calculated for each couple of delineation teams, and this per-imaging modality is described in Table 1. A Wilcoxon matched-pairs, signed-rank test was performed to compare the observer variability (overlap%, DSC, and MDA) between the bpMRI and PSMA PET-based contours. A Mann-Whitney U test was performed to compare the observer variability between the ^{68}Ga-PSMA PET and ^{18}F-PSMA PET subcohorts. Furthermore, to get better insight into the PSMA PET-based contours, the distribution of the SUV% for the $GTV^{majority}$, the $GTV^{minority}$, and the whole prostate gland was determined. A Kruskal-Wallis test was performed to assess SUV% distribution differences between the tracers used, and the median patientwise SUV% contrast ratio (SUV%-CR, calculated as median $GTV^{majority}$ SUV% / median prostate gland without $GTV^{majority}$ SUV%) was calculated according to the used radioligand. The significance level was defined as $P < .05$. Data were analyzed using MATLAB and SPSS for Windows, version 26.0 (IBM Corp, Armonk, New York).

Results

The characteristics of 19 of the 20 included patients are depicted in Table 2. One patient in the ^{68}Ga-PSMA group was excluded for further analysis because quantification of PET with SUV was not reliable owing to partial paravenous tracer injection. The median (IQR) histopathologically measured tumor volume was 5.0 (2.9-6.7) mL. Matching of both subcohorts (^{68}Ga-PSMA-11 and ^{18}F-PSMA-1007) was checked based on the resection specimen for tumor volume (^{68}Ga-PSMA vs ^{18}F-PSMA: median [IQR] volume, 5.0 [3.7-6.9] mL vs 4.6 [2.4-6.3] mL), ISUP grade (^{18}F-PSMA ≥ ISUP grade 3 for all except 1), and T-category (for ^{68}Ga-PSMA, 2 of 9 were pT2 and 7 of 9 were ≥pT3a; for ^{18}F-PSMA, 3 of 10 were pT2 and 7 of 10 were ≥pT3a). The 19 cases were distributed among the 4 delineation teams for both imaging modalities, leading to 76 delineations for bpMRI and 76 for PSMA PET. The index lesion as identified by histology was not detected or not located within the delineated volume in 6.6% (5 of 76) of the delineations by bpMRI, in 11.1% (4 of 36) of the delineations by ^{68}Ga-

Table 2 Patient data*

Patient	Scan information		Clinical information				Pathology information		
	Tracer	Time to acquisition (min)	ISUP grade (biopsy)	T category (MRI)	iPSA (ng/mL)	ISUP grade (specimen)	T category (specimen)	Tumor volume (mL)	Prostate volume (mL)
1	^{68}Ga	64	3	4	8.4	3	3a	6.9	76.7
2	^{68}Ga	67	2	3a	8.8	3	3a	5.0	71.4
3	^{68}Ga	75	4	2a	10.8	3	2	3.7	55.2
4	^{68}Ga	74	2	3a	21.0	3	3b	4.0	57.1
5	^{68}Ga	67	3	2c	3.8	5	3a	2.3	27.7
6	^{68}Ga	56	5	2a	24.6	5	2	3.3	55.0
7	^{68}Ga	60	2	3a	10.1	3	3b	5.6	35.0
8	^{68}Ga	71	4	3b	4.2	5	3b	11.0	22.0
9	^{68}Ga	78	5	3a	20.9	3	3b	28.2	51.3
10	^{18}F	62	3	2c	4.8	5	3a	2.2	56.4
11	^{18}F	59	5	2a	6.2	5	2	1.2	37.5
12	^{18}F	62	5	3a	6.4	5	3b	5.0	28.7
13	^{18}F	64	3	2b	5.3	2	3a	9.5	30.1
14	^{18}F	61	3	3b	11.6	3	3b	9.1	33.0
15	^{18}F	60	5	3a	16.6	5	3a	4.1	38.3
16	^{18}F	60	2	3a	2.1	5	3a	5.8	45.3
17	^{18}F	61	4	3a	12.3	3	2	2.4	30.4
18	^{18}F	69	3	2a	4.3	5	2	2.5	47.2
19	^{18}F	62	5	2c	27.5	3	3a	6.4	53.3

Abbreviations: ^{18}F = Fluorine-18; ^{68}Ga = Gallium-68; iPSA = initial prostate-specific antigen; ISUP = International Society of Urologic Pathology; MRI = magnetic resonance imaging; T category = tumor category.

* The clinical information was available to the observers. The pathology information was derived from the prostatectomy specimens.

PSMA PET, in 2.5% (1 of 40) of the delineations by ^{18}F-PSMA PET, in 1.3% (1 of 76) of the delineations by the union contour (0 of 36 ^{68}Ga-PSMA [0%] and 1 of 40 ^{18}F-PSMA [2.5%]), and in 13.2% (10 of 76) of the delineations by the intersection contour (6 of 36 ^{68}Ga-PSMA [16.7%] and 4 of 40 ^{18}F-PSMA [10.0%]). On bpMRI, none of the 4 teams detected the lesion in patient 18 and 1 team did not detect it in patient 19, whereas the nondetection of index lesions in the PSMA PET cohort was spread over 4 patients (2 teams did not detect the lesion in patient 3 [^{68}Ga-PSMA]; 1 team did not detect the lesion in patient 1 [^{68}Ga-PSMA]; 1 team did not detect the lesion in patient 5 [^{68}Ga-PSMA]; and 1 team did not detect the lesion in patient 18 [^{18}F-PSMA]). The median spatial overlap per team ranged from 38.9% to 55.9% for the bpMRI-based GTV contours, from 24.5% to 42.7% for the ^{68}Ga-PSMA PET-based contours, and from 57.0% to 75.1% for the ^{18}F-PSMA PET-based contours. Furthermore, a statistically significant difference in spatial overlap favoring PSMA PET-based delineations compared with bpMRI-based delineations was found in the ^{18}F-PSMA subgroup (median, 63.0% vs 53.1%; P = .004) but not in the ^{68}Ga-PSMA subgroup (median, 32.5% vs 50.6%; P = .100). The median GTV per team ranged from 2.7 mL to 3.9 mL for the bpMRI-based contours, from 2.6 mL to 3.5 mL for the ^{68}Ga-PSMA PET-based contours, and from 2.1 mL to 10.8 mL for the ^{18}F-PSMA PET-based contours. Detailed information about the different contour volumes is provided in Table 3.

Regarding the interobserver variability, a moderate agreement was observed for bpMRI-based delineations, with a median (IQR) DSC of 0.63 (0.37-0.69) and a median (IQR) MDA of 1.76 (1.25-3.60) mm. For the PSMA PET-based delineations, a median (IQR) DSC of 0.67 (0.43-0.79) was reached, with a median (IQR) MDA of 1.73 (0.92-4.00) mm. A detailed listing of the different GTV delineation strategies and their corresponding measures of interobserver variability is depicted in Table 4. Pairwise comparisons of the interobserver measurements showed a statistically significantly higher DSC for the PSMA PET-based delineations compared with the bpMRI-based contours (P = .015), with a median pairwise difference of 0.07. There was no statistically significant difference in MDA when both strategies were compared (P = .319).

In a tracer-based subanalysis (^{68}Ga-PSMA vs ^{18}F-PSMA), a median (IQR) DSC of 0.58 (0.26-0.77) with a median (IQR) MDA of 2.44 (1.10-5.48) mm was found for the ^{18}F-PSMA-based delineations (n = 10). For the ^{68}Ga-PSMA-based delineations (n = 9), a median (IQR) DSC of 0.72 (0.57-0.80) with a median (IQR) MDA of 1.22 (0.82-1.99) mm was found (Table 4). The measured DSCs (P = .019) and calculated MDAs (P = .003) were statistically significantly lower and higher, respectively, for the ^{18}F-PSMA cohort. To rule out inherent differences

Table 3 Teamwise gross tumor volumes and spatial overlap

	bpMRI			PSMA PET			PSMA PET/bpMRI	
	All (n = 19)	^{68}Ga-PSMA (n = 9)	^{18}F-PSMA (n = 10)	All (n = 19)	^{68}Ga-PSMA (n = 9)	^{18}F-PSMA (n = 10)	Union (n = 19)	Intersection (n = 19)
Median (IQR) spatial overlap, %								
Team 1	53.2 (35.4-60.5)	52.0 (34.5-61.7)	55.0 (37.9-65.2)	40.7 (18.1-62.1)	25.9 (18.8-45.4)	59.8 (19.1-62.8)	66.4 (54.0-69.8)	24.5 (13.1-37.2)
Team 2	51.2 (21.8-60.5)	51.4 (39.3-59.4)	50.8 (15.4-60.9)	53.9 (31.7-66.1)	38.0 (31.7-53.9)	57.0 (43.1-71.4)	67.3 (53.0-77.4)	32.3 (17.4-38.8)
Team 3	38.9 (20.8-53.4)	38.7 (21.1-43.9)	52.5 (15.4-59.6)	60.9 (39.8-75.1)	42.7 (23.5-50.8)	75.1 (71.0-87.8))	67.0 (52.2-84.3)	30.7 (11.2-37.9)
Team 4	55.9 (41.4-64.1)	60.8 (42.3-64.1)	52.2 (33.0-59.5)	50.5 (20.6-71.5)	24.5 (18.8-31.2)	71.2 (50.5-81.1)	64.0 (56.9-76.3)	28.5 (12.7-41.5)
Median (IQR) GTV, mL								
Team 1	3.3 (1.2-5.7)	3.7 (1.1-9.2)	2.0 (1.2-3.6)	2.3 (1.4-4.6)	2.6 (2.0-4.5)	2.1 (1.1-4.7)	4.3 (2.7-7.5)	1.0 (0.5-2.2)
Team 2	2.7 (1.1-5.1)	5.1 (1.3-6.6)	1.6 (0.6-3.6)	5.3 (3.3-7.0)	3.5 (3.1-5.7)	6.1 (4.9-7.6)	6.8 (4.7-9.0)	1.9 (0.5-2.2)
Team 3	3.0 (1.4-4.5)	3.9 (3.0-4.7)	2.4 (1.2-3.0)	5.9 (2.2-12.2)	3.3 (1.9-5.9)	10.8 (6.0-18.6)	7.7 (5.1-12.9)	2.0 (0.7-3.2)
Team 4	3.9 (1.7-6.1)	5.3 (3.9-6.1)	2.2 (1.1-5.5)	3.9 (1.2-8.9)	2.6 (1.2-4.1)	5.6 (1.7-14.3)	6.3 (3.0-9.4)	1.4 (0.6-2.2)

Abbreviations: ^{18}F = fluorine-18; ^{68}Ga = gallium-68; bpMRI = biparametric magnetic resonance imaging; GTV = gross tumor volume; IQR = interquartile range; PET = positron emission tomography; PSMA = prostate-specific membrane antigen.
The medians and IQRs for the GTVs and median spatial overlap with the coregistered histopathologic index lesion are shown teamwise. The bpMRI and PSMA PET delineations were divided in 2 subgroups for further analysis according to the tracer used (^{68}Ga-PSMA-11 or ^{18}F-PSMA-1007). The PSMA PET/bpMRI-based union volume (bpMRI ∪ PSMA PET) and intersection volume (bpMRI ∩ PSMA PET) were created.

Table 4 Interobserver variability characteristics according to the image modality used

	bpMRI	PSMA PET	^{68}Ga-PSMA (n = 9)	^{18}F-PSMA (n = 10)
	All (n = 19)	All (n = 19)		
Sørensen-Dice coefficient				
Median	0.63	0.67	0.72	0.58
Interquartile range	0.37-0.69	0.43-0.79	0.57-0.80	0.26-0.78
Mean	0.54	0.59	0.67	0.54
Standard deviation	0.24	0.24	0.19	0.26
Mean distance to agreement, mm				
Median	1.76	1.73	1.22	2.44
Interquartile range	1.25-3.60	0.92-4.00	0.82-1.99	1.10-5.48
Mean	3.83	2.93	1.81	3.74
Standard deviation	5.19	3.02	1.76	3.45

Abbreviations: ^{18}F = fluorine-18; ^{68}Ga = gallium-68; bpMRI = biparametric magnetic resonance imaging; PET = positron emission tomography; PSMA = prostate-specific membrane antigen.

of the tumor characteristics among both subcohorts, the same parameters for the bpMRI-based contours were compared between both subcohorts (^{68}Ga-PSMA vs ^{18}F-PSMA) as well. No statistically significant differences were observed for the bpMRI-based contours (DSC, P = .198; MDA, P = .855).

The SUV% distribution over the entire matched T2w-MRI delineated prostate gland[21] and the minority- and majority-voted PSMA PET-based GTV was determined to explore the observed difference in delineation behavior according to the tracer used. No significant difference in SUV% distribution was found for the GTV^{majority} contours when comparing the ^{68}Ga-PSMA-based delineations with the ^{18}F-PSMA-based contours (P = .207). However, the SUV% distribution in the whole prostate gland was significantly different in the ^{18}F-PSMA images compared with the ^{68}Ga-PSMA images (P < .001): a wide plateau of the whole prostate gland SUV% distribution curve was observed in the intermediate SUV% range for ^{18}F-PSMA, whereas the majority of the voxels in the ^{68}Ga-PSMA images were situated in the low SUV % range (Fig 1). Furthermore, the minority-voted, or "doubtful," GTV SUV% distribution showed that the bulk of doubtful voxels was situated in the intermediate SUV% range on the PSMA images with substantially more ^{18}F-PSMA doubtful voxels than ^{68}Ga-PSMA doubtful voxels (Fig 1). This was reflected by a median (IQR) patientwise SUV%-CR of 1.8 (1.6 -2.7) for the ^{18}F-PSMA images and 3.3 (2.7-5.9) for the ^{68}Ga-PSMA PET images (Fig 2).

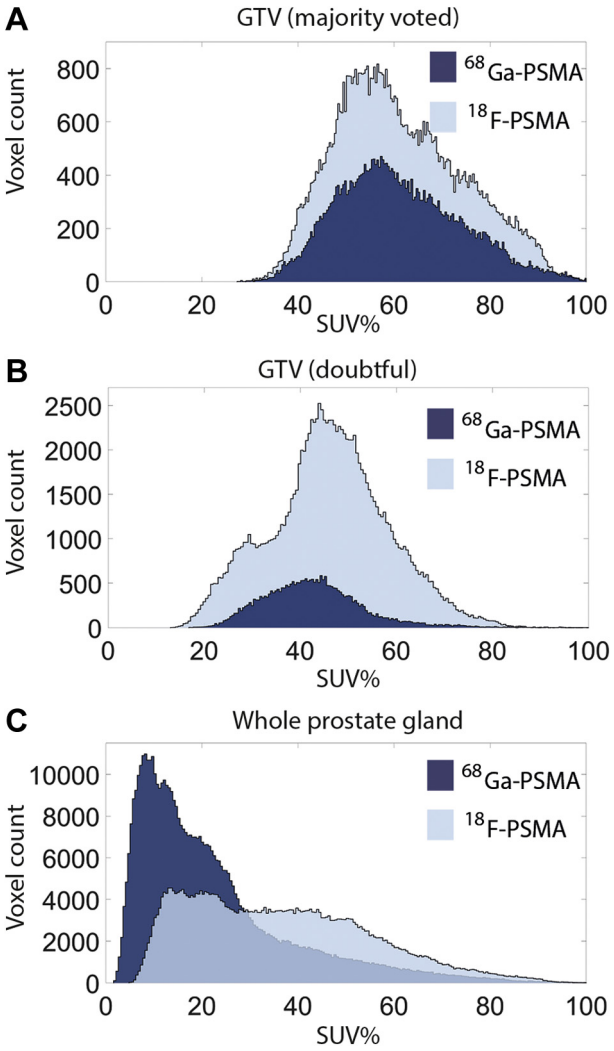

Figure 1 SUV% distribution histogram for ^{68}Ga-PSMA-11 versus ^{18}F-PSMA-PSMA-1007. (A) The SUV% distribution for the GTV^{majority} is plotted for both tracers. (B) The SUV% distribution for the "doubtful," minority-voted, GTV. (C) The SUV % distribution for the whole prostate gland is plotted. A significantly different SUV% distribution was found for the whole prostate gland ($P < .001$), but not for the majority-voted GTV ($P = .207$), by performing a Kruskal-Wallis test. A larger number of doubtful voxels was found for the ^{18}F-PSMA-based GTVs compared with the ^{68}Ga-PSMA-based GTVs, situated in the intermediate SUV% range. *Abbreviations:* ^{18}F = fluorine-18; ^{68}Ga = gallium-68; GTV = gross tumor volume; SUV = standardized uptake value.

Discussion

We investigated the accuracy and interobserver variability of delineating prostate index tumors on PSMA PET imaging compared with bpMRI imaging, the currently standard imaging modality used for GTV delineation in multiple clinical trials on focal boosting for PCa.[4,5,16,22-24] The bpMRI-based, ^{68}Ga-PSMA PET-based, and ^{18}F-PSMA PET-based delineation methods resulted in a nondetection rate of 6.6%, 11.1%, and 1.1%, respectively. A wider spread of nondetection across different patients was seen for the PSMA PET-based delineations compared with the bpMRI-based contours. The PSMA PET-based nondetections were spread across 4 different patients, whereas for the bpMRI-based delineations, the nondetections were found in only 2 patients; for 1 of the 19 included patients, none of the teams could accurately detect the index lesion. Regarding the PSMA PET-based nondetections (5 of 76), an imbalance in nondetection was noticed between the ^{68}Ga-PSMA subgroup (4 of 5) and the ^{18}F-PSMA subgroup (1 of 5). When applying a union (bpMRI ∪ PSMA PET) GTV, the pathologic index lesion was missed in only 1 case out of 76 delineations. These findings on target detection confirmed the previous findings of Zamboglou et al and Bettermann et al.[10,11] They showed that the highest sensitivity and spatial overlap can be reached using the union (bpMRI ∪ PSMA PET) GTV delineations compared with PSMA PET and bpMRI-based GTV delineations at the cost of a decreased delineation specificity. Nevertheless, the data from this study indicate that a combined use and interpretation of both imaging modalities results in increased detection of index lesions.

When focusing on the spatial overlap between the GTV delineation and the pathologically defined index lesion, no general improved spatial overlap was found for either bpMRI-based or PSMA PET-based GTV delineations, compared with each other. These findings are congruent with the results published by Zamboglou et al, who used ^{68}Ga-PSMA.[10] However, based on our tracer-dependent subgroup analysis, the ^{18}F-PSMA subgroup clearly showed the highest median spatial overlap with the histopathologically defined index lesion for each delineation team separately. The median histopathologically measured tumor volume (5.0 mL) was larger than the median delineated GTV by all teams for the bpMRI-based contours (2.7-3.3 mL). The median delineated PSMA PET-based GTV per team was between 2.3 and 5.9 mL. These results are in line with the earlier findings that MRI-based contours underestimate in general the tumor burden.[11,25-27] An option to improve tumor covering by MRI-based focal boosting might be the adoption of a safety margin in terms of a clinical target volume. Furthermore, we suggest maintaining a sufficient radiation therapy dose to the whole prostate gland to prevent undertreatment of undetected tumor regions in focal radiation therapy strategies for high- and intermediate-risk patients with PCa.

A moderate but acceptable variability between the different delineation teams was shown for both the PSMA PET-based and bpMRI-based contours, with median MDAs of 1.73 mm and 1.76 mm, respectively. Pairwise MDA was determined to compare agreement in absolute terms, independent of volume, as DSC is more forgiving

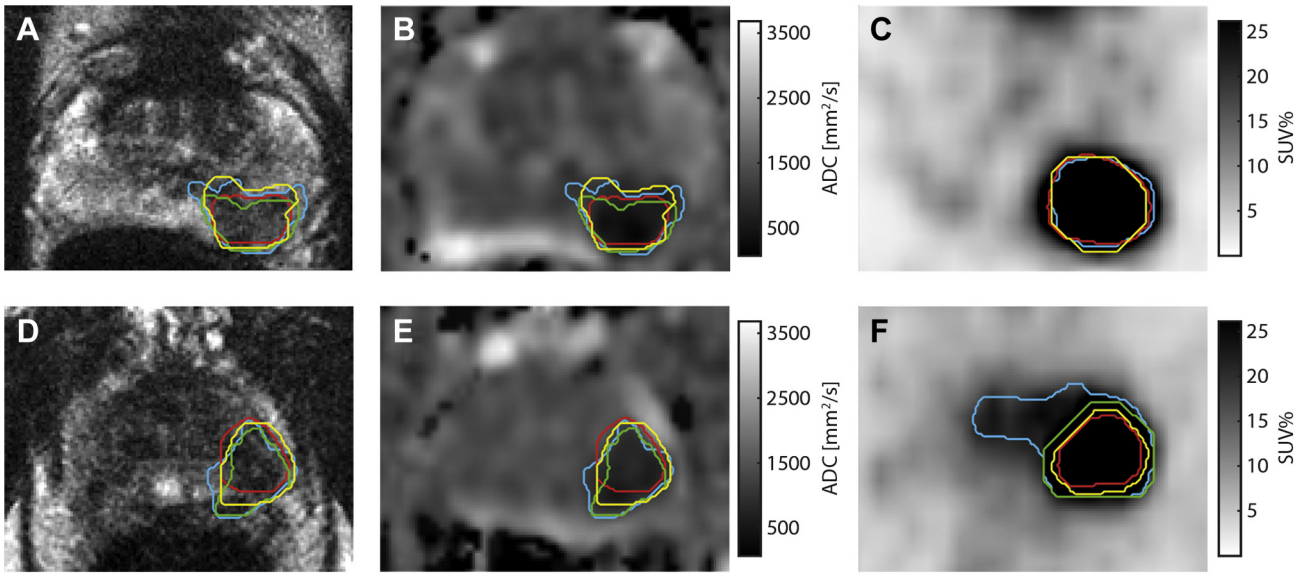

Figure 2 Example of delineations by the 4 teams on T2 weighted images (A, D), ADC images (B, E), and PSMA PET images (C, F) for one ^{68}Ga-PSMA PET/MRI patient (A, B, and C) and one ^{18}F-PSMA PET/MRI patient (D, E, and F). Comparing the ^{68}Ga-PSMA PET image (C) with the ^{18}F-PSMA PET image (F), the difference between both in patientwise SUV%-CR is visualized. *Abbreviations:* ADC = apparent diffusion coefficient; CR = contrast ratio; MRI = magnetic resonance imaging; PET = positron emission tomography; PSMA = prostate-specific membrane antigen; SUV = standardized uptake value.

for the same absolute error for larger volumes than for smaller volumes. Because the statistically significant difference in DSC between both modalities (ie, favoring PSMA PET-based delineations) is not reflected in a statistically significant MDA difference, this difference will hardly be reflected in the target volume contour and will, therefore, have only limited clinical relevance regarding the aimed radiation dose distribution.

To our knowledge, we are the first research group to investigate differences in delineation outcome according to the tracer used for PSMA PET-based GTV contouring in PCa. Previous studies on PSMA PET-based GTV delineation for focal boosting in PCa were performed using ^{68}Ga-PSMA-11 as the tracer.[7,10-12] Kuten et al[28] performed a head-to-head comparison between ^{68}Ga-PSMA-11 and ^{18}F-PSMA-1007 PET/CT, showing similar outcomes regarding the identification of dominant intraprostatic lesions for both tracers. Furthermore, they found that the use of ^{18}F-PSMA-1007 as the tracer leads to the detection of additional low-grade lesions of limited clinical relevance.[28] However, their study focused mainly on diagnostic rather than contouring aspects of PSMA PET imaging. In this study, we demonstrated a lower nondetection rate and higher median spatial overlap for ^{18}F-PSMA PET-based GTV delineations compared with the ^{68}Ga-PSMA PET-based contours. The higher index-lesion detection rate and spatial overlap volumes for the ^{18}F-PSMA PET-based delineations were in tandem with generally larger GTVs and lower interobserver agreement. We analyzed and compared the PSMA PET images obtained by using both tracers in depth to explain the mentioned differences. A similar SUV% distribution in the majority-voted GTVs was observed for both tracers. However, a different SUV% distribution was found within the whole prostate gland. This altered SUV% distribution throughout the prostate gland with more voxels situated in the intermediate SUV% range leads to a more difficult distinction of voxels that are very likely tumoral from those that are very unlikely tumoral. This hypothesis was enhanced by the larger number of doubtful voxels found for the ^{18}F-PSMA-based GTVs compared with the ^{68}Ga-PSMA-based GTVs, situated in the intermediate SUV% range. This finding could be responsible for the larger delineated GTVs, the higher spatial overlap volumes, and the increased interobserver variability found for ^{18}F-PSMA PET-based delineations. Recently, Zamboglou et al showed that for ^{68}Ga-PSMA PET-based delineations, the use of similar window levels reduces interobserver variability. They recommended the use of a minimum SUV of 0 to a maximum of 5 as PET image scaling for ^{68}Ga-PSMA PET-based manual delineations.[12] It might be possible that predefined optimal window levels could lead to an increase in interobserver agreement for ^{18}F-PSMA PET-based delineations as well, but this is yet to be confirmed. Hence, the window-level selection used in this study was at the discretion of the delineating physician to avoid favoring 1 tracer over the other.

The main limitation of this study is the existing uncertainty regarding the correlation of the PET/MRI data and histopathology data, including a nonlinear shrinkage of the whole prostate gland after prostatectomy.[29] In

addition, the apex and base of the prostate are missing for registration because of the required dedicated pathologic processing of these zones; however, by reporting and comparing spatial overlap volumes after a deformable point-based registration, this limitation is reduced to a minimum. To obtain a perfect comparison of both tracers, we would have to scan each patient twice (^{68}Ga-PSMA-11 and ^{18}F-PSMA-1007), but owing to the balanced spread of the patient populations between both subcohorts and the availability of bpMRI data as a benchmark, we were able to reliably compare both tracers. A third limitation may be the use of bpMRI as an alternative to multiparametric MRI for delineation. However, given that dynamic contrast-enhanced MRI has a secondary role to T2w and DWI in the detection of PCa, the use of bpMRI for radiation therapy purposes is gaining ground.[30] To assess the value of combined bpMRI and PET information, we had to opt for union and intersection contours. Achieving consensus contours between the radiologist, nuclear medicine physician, and radiation oncologist turned out to be not feasible because of the diversity in information present in both images. Finally, a selection bias was caused by enrolling only high-risk and intermediate-risk patients with PCa who were scheduled for prostatectomy. As a result, our findings are strictly applicable to these risk groups only.

Conclusions

This study showed a nondetection rate of 6.6%, 11.1%, and 1.1% for bpMRI-based, ^{68}Ga-PSMA PET-based, and ^{18}F-PSMA PET-based delineations, respectively. In a subanalysis focusing on the PSMA tracer used, we found an altered SUV distribution in the whole prostate gland for ^{18}F-PSMA-based images compared with ^{68}Ga-PSMA-based images, resulting in increased interobserver variability for the ^{18}F-PSMA PET delineations. However, the ^{18}F-PSMA PET delineations were in general associated with a higher index-lesion detection rate and a higher spatial overlap with the pathologically defined index lesion. Taking into account these findings, there is a need to develop specific, tracer-dependent, window-level guidelines for GTV contouring for focal boosting purposes.

Acknowledgments

The authors thank the team of Kim Serdons for production of ^{68}Ga-PSMA-11 and ^{18}F-PSMA-1007; Kwinten Porters and Jef Van Loock for performing PSMA PET/MRI acquisitions; and Lotte Lutkenhaus, Laurence Delombaerde, and Kenneth Poels for their efforts in the data transfer and IT support.

Supplementary Materials

Supplementary material for this article can be found at https://doi.org/10.1016/j.prro.2020.11.006.

References

1. Agarwal PK, Sadetsky N, Konety BR, et al. Treatment failure after primary and salvage therapy for prostate cancer. *Cancer*. 2008;112:307-314.
2. Quero L, Vercellino L, de Kerviler E, et al. 18F-choline PET/CT and prostate MRI for staging patients with biochemical relapse after irradiation for prostate cancer. *Clin Nucl Med*. 2015;40:e492-e495.
3. Cellini N, Morganti AG, Mattiucci GC, et al. Analysis of intraprostatic failures in patients treated with hormonal therapy and radiotherapy: Implications for conformal therapy planning. *Int J Radiat Oncol*. 2002;53:595-599.
4. Lips IM, van der Heide UA, Haustermans K, et al. Single blind randomized phase III trial to investigate the benefit of a focal lesion ablative microboost in prostate cancer (FLAME-trial): Study protocol for a randomized controlled trial. *Trials*. 2011;12:255.
5. Murray JR, Tree AC, Alexander E, et al. Standard and hypofractionated dose escalation to intraprostatic tumour nodules in localised prostate cancer: Efficacy and toxicity in the DELINEATE trial. *Int J Radiat Oncol*. 2020;106:715-724.
6. Eiber M, Weirich G, Holzapfel K, et al. Simultaneous 68Ga-PSMA HBED-CC PET/MRI improves the localization of primary prostate cancer. *Eur Urol*. 2016;70:829-836.
7. Zamboglou C, Schiller F, Fechter T, et al. 68 Ga-HBED-CC-PSMA PET/CT versus histopathology in primary localized prostate cancer: A voxel-wise comparison. *Theranostics*. 2016;6:1619-1628.
8. Fendler WP, Schmidt DF, Wenter V, et al. 68Ga-PSMA PET/CT detects the location and extent of primary prostate cancer. *J Nucl Med*. 2016;57:1720-1725.
9. Rhee H, Thomas P, Shepherd B, et al. Prostate specific membrane antigen positron emission tomography may improve the diagnostic accuracy of multiparametric magnetic resonance imaging in localized prostate cancer. *J Urol*. 2016;196:1261-1267.
10. Zamboglou C, Drendel V, Jilg CA, et al. Comparison of 68Ga-HBED-CC PSMA-PET/CT and multiparametric MRI for gross tumour volume detection in patients with primary prostate cancer based on slice by slice comparison with histopathology. *Theranostics*. 2017;7:228-237.
11. Bettermann AS, Zamboglou C, Kiefer S, et al. [68Ga-]PSMA-11 PET/CT and multiparametric MRI for gross tumor volume delineation in a slice by slice analysis with whole mount histopathology as a reference standard—Implications for focal radiotherapy planning in primary prostate cancer. *Radiother Oncol*. 2019;141:214-219.
12. Zamboglou C, Fassbender TF, Steffan L, et al. Validation of different PSMA-PET/CT-based contouring techniques for intraprostatic tumor definition using histopathology as standard of reference. *Radiother Oncol*. 2019;141:208-213.
13. Briganti A, Larcher A, Abdollah F, et al. Updated nomogram predicting lymph node invasion in patients with prostate cancer undergoing extended pelvic lymph node dissection: The essential importance of percentage of positive cores. *Eur Urol*. 2012;61:480-487.
14. Van Binnebeek S, Vanbilloen B, Baete K, et al. Comparison of diagnostic accuracy of 111In-pentetreotide SPECT and 68Ga-DOTATOC PET/CT: A lesion-by-lesion analysis in patients with metastatic neuroendocrine tumours. *Eur Radiol*. 2016;26:900-909.
15. Monninkhof EM, van Loon JWL, van Vulpen M, et al. Standard whole prostate gland radiotherapy with and without lesion boost in

prostate cancer: Toxicity in the FLAME randomized controlled trial. *Radiother Oncol*. 2018;127:74-80.
16. Draulans C, Heide UA Van Der, Haustermans K, et al. Primary endpoint analysis of the multicentre phase II hypo-FLAME trial for intermediate and high risk prostate cancer. *Radiother Oncol*. 2020; 147:92-98.
17. Brierley J, Gospodarowicz MK, Wittekind C. *TNM classification of malignant tumours*. Chichester, West Sussex, UK: Wiley-Blackwell Publishing Ltd.; 2017.
18. Epstein JI, Egevad L, Amin MB, et al. The 2014 International Society of Urological Pathology (ISUP) consensus conference on Gleason grading of prostatic carcinoma: Definition of grading patterns and proposal for a new grading system. *Am J Surg Pathol*. 2016;40:244-252.
19. Liu W, Laitinen S, Khan S, et al. Copy number analysis indicates monoclonal origin of lethal metastatic prostate cancer. *Nat Med*. 2009;15:559-565.
20. Ahmed HU. The index lesion and the origin of prostate cancer. *N Engl J Med*. 2009;361:1704-1706.
21. Salembier C, Villeirs G, De Bari B, et al. ESTRO ACROP consensus guideline on CT- and MRI-based target volume delineation for primary radiation therapy of localized prostate cancer. *Radiother Oncol*. 2018;127:49-61.
22. Aluwini S, van Rooij P, Hoogeman M, et al. Stereotactic body radiotherapy with a focal boost to the MRI-visible tumor as monotherapy for low- and intermediate-risk prostate cancer: Early results. *Radiat Oncol*. 2013;8:84.
23. Herrera FG, Valerio M, Berthold D, et al. 50 Gy stereotactic body radiation therapy to the dominant intra-prostatic nodule: Results from a phase Ia/b trial. *Int J Radiat Oncol Biol Phys*. 2019;103:320-334.
24. Draulans C, De Roover R, van der Heide UA, et al. Stereotactic body radiation therapy with optional focal lesion ablative microboost in prostate cancer: Topical review and multicenter consensus. *Radiother Oncol*. 2019;140:131-142.
25. Panebianco V, Giganti F, Kitzing YX, et al. An update of pitfalls in prostate mpMRI: A practical approach through the lens of PI-RADS v. 2 guidelines. *Insights Imaging*. 2018;9:87-101.
26. Steenbergen P, Haustermans K, Lerut E, et al. Prostate tumor delineation using multiparametric magnetic resonance imaging: Inter-observer variability and pathology validation. *Radiother Oncol*. 2015;115:186-190.
27. Johnson D, Raman S, Mirak S, et al. Detection of individual prostate cancer foci via multiparametric magnetic resonance imaging. *Eur Urol*. 2019;75:712-720.
28. Kuten J, Fahoum I, Savin Z, et al. Head-to-head comparison of 68Ga-PSMA-11 with 18F-PSMA-1007 PET/CT in staging prostate cancer using histopathology and immunohistochemical analysis as a reference standard. *J Nucl Med*. 2020;61: 527-532.
29. Schned AR, Wheeler KJ, Hodorowski CA, et al. Tissue-shrinkage correction factor in the calculation of prostate cancer volume. *Am J Surg Pathol*. 1996;20:1501-1506.
30. Alabousi M, Salameh J-P, Gusenbauer K, et al. Biparametric vs multiparametric prostate magnetic resonance imaging for the detection of prostate cancer in treatment-naïve patients: A diagnostic test accuracy systematic review and meta-analysis. *BJU Int*. 2019; 124:209-220.